Supplementary Information

Role of noncollinear spin texture driven z-torque in deterministic spin-orbit torque induced switching of perpendicular magnetization

Suhyeok An[1], Hyeong-Joo Seo[1,†], Dongryul Kim[1], Ki-Seung Lee[2], Eunchong Baek[1], Jun-Su Kim[1], Soobeom Lee[3], Chun-Yeol You[1,*]

[1] Department of Physics and Chemistry, DGIST, Daegu 42988, South Korea

[2] Emerging Materials Science Research Center, DGIST, Daegu 42988, South Kore

[3] Center for Basic Science, DGIST, Daegu 42988, South Korea

[*] Correspondence to cyyou@dgist.ac.kr

[†] Present address: Department of Materials Science and Engineering, KAIST, Daejeon 34141, South Korea

Contents

Note I. System energy evaluation depending on the type of chirality of noncollinear spin texture.

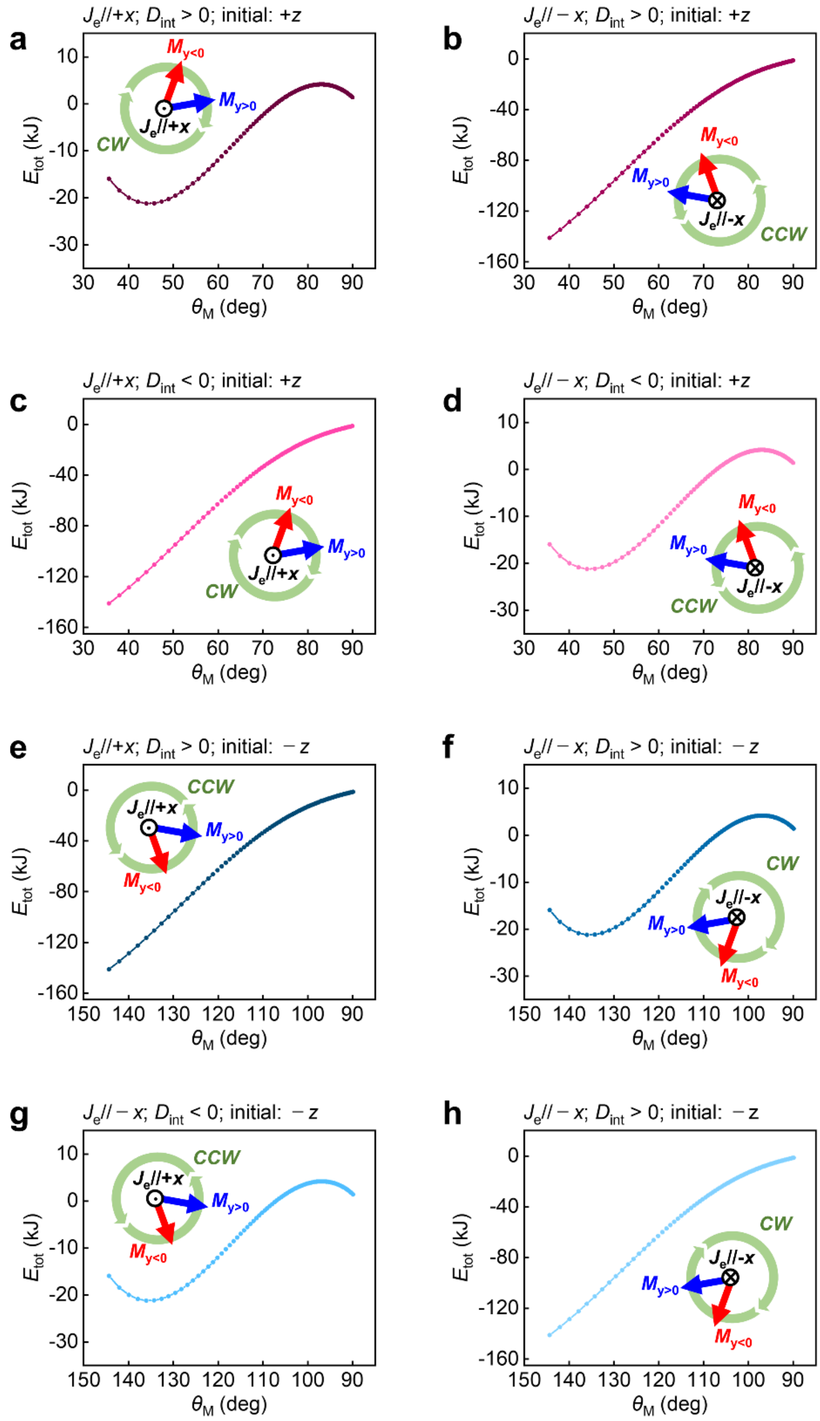

Fig. S1. E_{tot} calculations according to initialization, J_e direction, and sign of D_{int} at **a,b,c,d** +*z* initialization and **e,f,g,h** -*z* initialization case. **a,c,e,g** J_e//+*x* and **b,d,f,h** J_e//-*x*. **a,b,e,f** $D_{\mathrm{int}} > 0$ and **c,d,g,h** $D_{\mathrm{int}} < 0$. In the whole figure, the schematic diagram of magnetization appears, and the chirality of spin texture is determined based on the spatial variation of magnetization distribution from -*y* to +*y* position.

The correlation between the chiral type of noncollinear spin texture (NST) and the sign of interfacial Dzyaloshinskii-Moriya interaction (DMI) energy density (D_{int}) plays a critical role in torque generation. In this context, the chiral type of NST is determined by the magnetization (M) initialization direction and the electric current (J_e) direction, while the sign of D_{int} is an intrinsic property established when the system is formed. We will define the chiral type considering all possible initialization and J_e directions and examine its correlation between the D_{int} sign and torque generation.

Suppose there exists lateral direction perpendicular magnetic anisotropy (PMA) symmetry breaking within the system. In this case, spin-orbit torque (SOT) injection can lead to the formation of NST. To make it easier to understand, we will use the notation (+*z*, +*x*) to represent the (M initialization direction, J_e direction). Fig. S1 illustrates the different chiral types, where (+*z*, +*x*) and (-*z*, -*x*) have the same chirality, while (+*z*, -*x*) and (-*z*, +*x*) have the same chirality but opposite direction with (+*z*, +*x*) and (-*z*, -*x*).

The reason for opposite chiral types of NST can be understood through schematic diagrams within each figure. In the case of +*z* initialization, where NST has $0 < M \leq 90$, M in $y < 0$ has higher PMA energy density, causing it to tilt less comparing with M in $y > 0$. When J_e is directed along +*x*, SOT aligns M in the +*y* direction, resulting in clockwise (CW) chirality. Conversely, when J_e is directed along -*x*, M aligns in the -*y* direction, leading to counter-clockwise (CCW) chirality. However, for -*z* initialization, the situation is entirely reversed. Here, NST has $90 \leq \mathrm{M} < 180$, which results in CCW chirality when J_e is directed along +*x* and CW chirality when Je is directed along -*x*. Therefore, (+*z*, +*x*) and (-*z*, -*x*) exhibit the same chiral type, as do (+*z*, -*x*) and (-*z*, +*x*).

However, it's essential to note that while NST have the same chiral type, what actually determines the system energy and torque is the interaction between DMI and NST. Even when systems exhibit the same chiral type as like Fig. S1a and Fig. S1c, a change in the sign of D_{int} results in the opposite energy change. This is similar to the change resulting from the difference in the chiral type of NST when D_{int} remains the same, Fig. S1a and Fig. S1b. It is because the sign of D_{int} determines the preferred chiral type of NST, resulting in different energy forms and torque distributions although the chirality of NST is same.[S1] It confirms that the chiral type of NST and the sign of D_{int} determine the system's torque direction, even when the initialization direction is reversed as seen in the comparison between Fig. S1e vs Fig. S1f and Fig. S1e vs Fig. S1g.

II. Position dependent magnetization angle distribution and torque calculation.

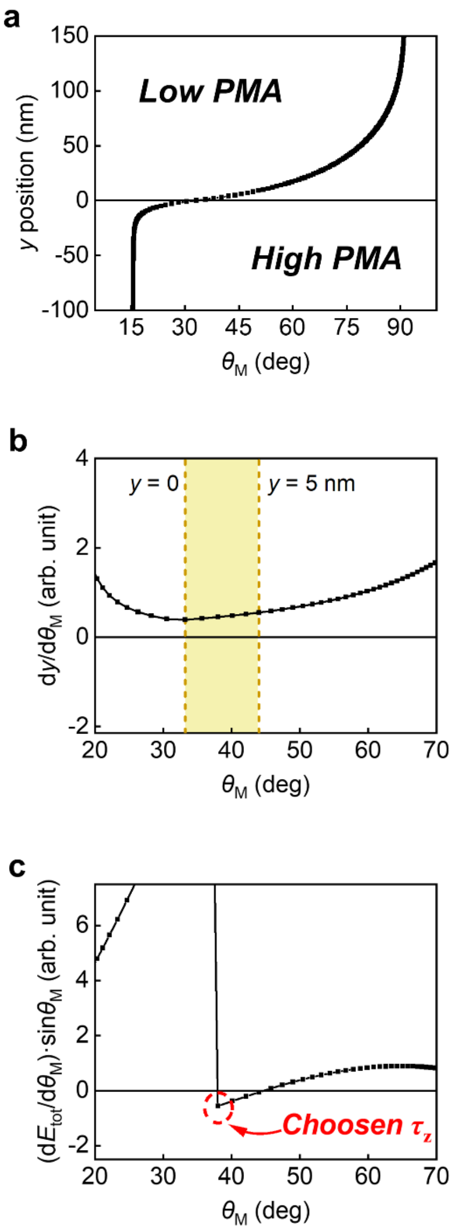

Fig. S2. **a** Graph about y position versus θ_M. **b** Calculated 1st derivative of y position about θ_M. Here, the yellow region indicates the range of negative slope in inset figure of Fig. 4a of main text and each dashed line is case of $y = 0$ and 5 nm, respectively. **c** Calculated z directional torque component (τ_z). The dashed circle indicates the example of determined τ_z for its tendency analysis in Fig. 5 of main text.

In Fig. 4 of the main text, we conducted y position dependent derivatives of E_{tot} to examine its relationship with spatial τ_z distribution. However, for actual torque calculations, we require angular derivatives of E_{tot}. And it is reason that we prepared this Note II. Fig. S2a illustrates the relationship between y position and θ_M. This relationship can be directly understood from Fig. 3d in the main text using the expression $m_z = \cos\theta_M$. As observed in the results, the high PMA region ($y < 0$) has a smaller degree of tilting compared to the low PMA region ($y > 0$). When you take the first derivative of this graph with respect to θ_M, the results indicate that the change in magnetization is primarily prominent in the regions where the change is abrupt, as shown in Fig. S2b, and all values are positive.

Therefore, based on the relationship of $dE_{tot}/d\theta_M = (dE_{tot}/dy) \cdot (dy/d\theta_M)$, we can speculate that the sign of the torque is determined solely by dE_{tot}/dy, and $dy/d\theta_M$ only affects its magnitude on torque. Thus, explanation of the sign of torque using only the spatial distribution as in Fig. 4 of the main text has no issue. Furthermore, we calculated τ_z by multiplying $\sin\theta_M$ with $dE_{tot}/d\theta_M$ to examine only the z component, as shown in Fig. S2c. Consequently, the calculated τ_z follows the sign trend determined by dE_{tot}/dy also. Here, we selected the τ_z with the most abrupt change for the analysis in Fig. 5 of the main text.

III. Evaluation of perpendicular magnetic anisotropy field varied from helium ion irradiation.

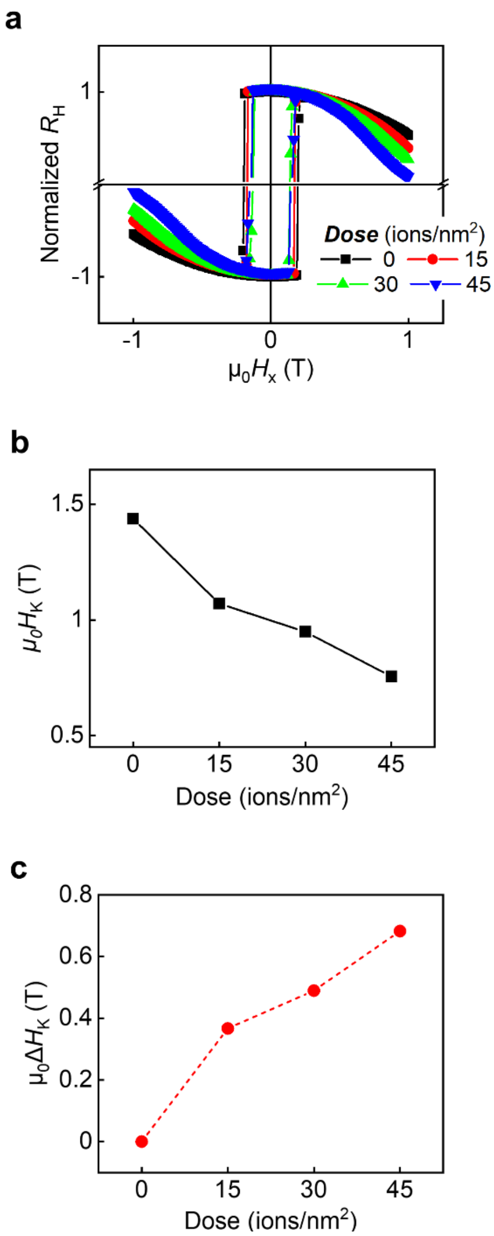

Fig. S3. Analysis of anisotropy characteristics by HII process. **a** AHE hysteresis loop under in-plane directional magnetic field according to dose. **b** Extracted H_K using GST method and **c** calculated ΔH_K. Here ΔH_K can be calculated by $\Delta H_K \equiv H_K^{NI} - H_K^{I}$ and H_K^{NI} is fixed to H_K at dose = 0 ions/nm^2.

The helium ion irradiation (HII) process can change magnetic properties such as the anisotropy properties,[S2-S4] exchange bias between FM/antiferromagnet interface,[S5-S7] DMI,[S8,S9] motion of domain wall (DW),[S10,S17] SOT properties,[S12-S15] and skyrmion manipulation.[S16,S17]. Among various changes observed in the experiment, we focus on PMA and DMI variations. But there was some reports that DMI is less sensitive to changes within an appropriate dose range compared to changes in [S8,S14,S16]. Therefore, the study ignored variations in DMI and instead focused on changes in PMA energy due to HII using the general Sucksmith-Thompson (GST) method for anisotropy analysis.[S18] For GST measurements, the anomalous Hall effect (AHE) hysteresis loop is requisite as shown in Fig. S3a with respect to the in-plane directional magnetic field. Measured hysteresis loop is able to fit with GST equation and Fig. S3b presents the results of extracting the effective anisotropy field (H_K). In here, we should mention that the measured H_K is effective anisotropy field considering the demagnetization contribution also. As observed, with increasing the degree of ion irradiation, denoted as dose, the anisotropy decreases significantly, with values of $\mu_0 H_K$ = 1.44, 1.07, 0.95, and 0.76 T for doses of 0, 15, 30, and 45 ions/nm^2, respectively. Importantly, the difference in H_K between the irradiated (I) region and the non-irradiated (NI) region, defined as $\Delta H_K \equiv H_K^{NI} - H_K^{I}$, is noteworthy. The calculated ΔH_K is shown in Fig. S3c, and it exhibits an increasing trend with dose. Specifically, at doses of 15, 30, and 45 ions/nm^2, $\mu_0 \Delta H_K$ = 0.4, 0.5, and 0.7 T, respectively.

References

S1. Yang, H., Thiaville, A., Rohart, S., Fert, A. & Chshiev, M. Anatomy of Dzyaloshinskii-Moriya Interaction at Co / Pt Interfaces. *Phys. Rev. Lett.* **115**, 267210 (2015).

S2. Chappert, C. *et al.* Planar Patterned Magnetic Media Obtained by Ion Irradiation. *Science* **280**, 1919–1922 (1998).

S3. Devolder, T. Light ion irradiation of Co/Pt systems: Structural origin of the decrease in magnetic anisotropy. *Phys. Rev. B* **62**, 5794–5802 (2000).

S4. Devolder, T. *et al.* Magnetic properties of He + -irradiated Pt/Co/Pt ultrathin films. *Phys. Rev. B* **64**, 064415 (2001).

S 5. Wang, C. *et al.* Defect-Induced Exchange Bias in a Single $SrRuO_3$ Layer. *ACS Appl. Mater. Interfaces* **10**, 27472–27476 (2018).

S6. Kuświk, P. *et al.* Tailoring Perpendicular Exchange Bias Coupling in Au/Co/NiO Systems by Ion Bombardment. *Nanomaterials* **8**, 813 (2018).

S7. Jensen, C. J. *et al.* Ion irradiation and implantation modifications of magneto-ionically induced exchange bias in Gd/NiCoO. *J. Magn. Magn. Mater.* **540**, 168479 (2021).

S8. Sud, A. *et al.* Tailoring interfacial effect in multilayers with Dzyaloshinskii–Moriya interaction by helium ion irradiation. *Sci. Rep.* **11**, 23626 (2021).

S9. Nembach, H. T. *et al.* Tuning of the Dzyaloshinskii–Moriya interaction by He+ ion irradiation. *J. Appl. Phys.* **131**, 143901 (2022).

S10. Diez, L. H. *et al.* Enhancement of the Dzyaloshinskii-Moriya interaction and domain wall velocity through interface intermixing in Ta/CoFeB/MgO. *Phys. Rev. B* **99**, 054431 (2019).

S11. Zhao, X. *et al.* Enhancing domain wall velocity through interface intermixing in W-CoFeB-MgO films with perpendicular anisotropy. *Appl. Phys. Lett.* **115**, 122404 (2019).

S12. Zhao, X. *et al.* Spin–orbit torque driven multi-level switching in He+ irradiated W–CoFeB–MgO

Hall bars with perpendicular anisotropy. *Appl. Phys. Lett.* **116**, 242401 (2020).

S13. Dunne, P. *et al.* Helium Ion Microscopy for Reduced Spin Orbit Torque Switching Currents. *Nano Lett.* **20**, 7036–7042 (2020).

S14. An, S., Baek, E., Kim, J.-A., Lee, K.-S. & You, C.-Y. Improved spin–orbit torque induced magnetization switching efficiency by helium ion irradiation. *Sci. Rep.* **12**, 3465 (2022).

S15. Lee, T. *et al.* Field-free spin-orbit torque switching of GdCo ferrimagnet with broken lateral symmetry by He ion irradiation. *Acta Mater.* **246**, 118705 (2023).

S16. Juge, R. *et al.* Helium Ions Put Magnetic Skyrmions on the Track. *Nano Lett.* **21**, 2989–2996 (2021).

S17. Kern, L.-M. *et al.* Deterministic Generation and Guided Motion of Magnetic Skyrmions by Focused He^+ -Ion Irradiation. *Nano Lett.* **22**, 4028–4035 (2022).

S18. Okamoto, S., Nishiyama, K., Kitakami, O. & Shimada, Y. Enhancement of magnetic surface anisotropy of Pd/Co/Pd trilayers by the addition of Sm. *J. Appl. Phys.* **90**, 4085–4088 (2001).